Structural, thermal and magnetic properties of $ErMn_2D_6$ synthesized under high deuterium pressure

2006 J. Phys.: Condens. Matter 18 6409

(http://iopscience.iop.org/0953-8984/18/27/023)

INSTITUTE OF PHYSICS PUBLISHING JOURNAL OF PHYSICS: CONDENSED MATTER

J. Phys.: Condens. Matter **18** (2006) 6409–6420 doi:10.1088/0953-8984/18/27/023

Structural, thermal and magnetic properties of $ErMn_2D_6$ synthesized under high deuterium pressure

V Paul-Boncour[1,7], S M Filipek[2], G André[3], F Bourée[3], M Guillot[4], R Wierzbicki[2], I Marchuk[2], R S Liu[5], B Villeroy[1], A Percheron-Guégan[1], H D Yang[6] and S C Pin[6]

[1] Laboratoire de Chimie Métallurgique des Terres Rares, CNRS, 2-8 rue H. Dunant, 94320 Thiais, France
[2] Institute of Physical Chemistry. PAN, Ulica Kasprzaka 44/52, 01224 Warsaw, Poland
[3] Laboratoire Léon Brillouin, CEA-CNRS, CEA/Saclay, 91191 Gif-sur-Yvette, France
[4] LCMI, CNRS-MPI, BP166, 38042 Grenoble Cedex 9, France
[5] Department of Chemistry, National Taiwan University, Taipei 106, Taiwan, Republic of China
[6] Department of Physics, National Sun Yat-Shen University, Kaoshiung 804, Taiwan, Republic of China

E-mail: paulbon@glvt-cnrs.fr

Received 13 April 2006
Published 23 June 2006
Online at stacks.iop.org/JPhysCM/18/6409

Abstract

A new phase of $ErMn_2D_6$ has been prepared by applying high hydrogen pressure on C14 $ErMn_2$. This phase is isostructural to YMn_2D_6 and crystallizes with a K_2PtCl_6 type structure having an ordered anion and a partially disordered cation arrangement as Er and half the Mn atoms are randomly substituted in the same 8c site. This hydride is very stable and decomposes into ErD_2 and Mn at about 630 K. The reverse susceptibility follows a Curie–Weiss law with an effective moment of 10 μ_B similar to that of $ErMn_2$. Although a saturation magnetization of 5 μ_B is measured at 4.2 K, smaller than that of $ErMn_2$ (8 μ_B), no long range magnetic order is observed in the neutron patterns. Short range magnetic order, corresponding to both ferromagnetic and antiferromagnetic correlations, is observed in the neutron patterns up to 5 K. The chemical disorder of Er and Mn atoms on the 8c site should prevent the long range magnetic order and favour a distribution of Er spin orientation.

1. Introduction

Hydrogen absorption in RMn_2 intermetallic compounds (R = rare earth) is known to modify significantly their magnetic properties. For hydrogen stoichiometries up to $x = 4.5$, the YMn_2H_x hydrides crystallize in a structure derived from that of the parent intermetallic, with H atoms located in tetrahedral interstitial sites and a continuous cell volume expansion [1–7].

[7] Author to whom any correspondence should be addressed.

Both hydrogen order and magnetic order occur below a transition temperature that increases with H content. The Mn moment is stabilized and the Mn–Mn magnetic interactions become stronger as the cell volume increases due to H absorption. The RMn_2 hydrides shows the same type of structural and magnetic phase diagram as YMn_2 hydride, with orientations of the R moments depending of the R anisotropy [8–10].

In order to determine if it is possible to obtain a YMn_2 hydride with a larger H content than $x = 4.5$, YMn_2 was submitted to a hydrogen pressure of several MPa. This method has already been successfully applied to synthesize novel hydrides of Laves phase compounds like YFe_2H_5 and $ErFe_2H_5$ [11, 12], which display interesting magnetic properties. We successfully prepared YMn_2H_6 [13, 14] which has a weight capacity of 3% comparable to that obtained in ZrV_2H_6 [15]. According to x-ray (XRD) and neutron powder diffraction (NPD) experiments, YMn_2D_6 crystallizes in a K_2PtCl_6 type structure with $a = 6.709(1)$ Å at 300 K. In the $Fm3m$ space group the Y and half of the Mn atoms (Mn1) randomly occupy the 8c site whereas the remaining Mn atoms (Mn2) are located in the 4a site and surrounded by 6 H atoms in the 24e site [13]. This structure is very different from that observed for the other YMn_2H_x hydrides (deuterides) ($0 < x \leqslant 4.5$) and is not derived from that of the parent intermetallic. As a matter of fact, the crystal structure of YMn_2H_6 results from a complete reorganization of the unit cell of the parent compound. Its structure is very close to that obtained for M_2TH_6 hydrides where M is an alkaline rare earth (Mg, Ca, Sr) or a divalent rare earth (Eu, Yb) and T a transition metal (Fe, Ru, Os) [16]. These hydrides are described as complex anions $(TH_6)^{4-}$ surrounded by a cage of divalent M^{2+} cations. The short distance between T and H atoms is indicative of covalent bonding. Therefore by analogy, YMn_2D_6 has to be considered rather as a complex hydride than as an interstitial metal hydride. Synthesis of the deuterated compounds showed for the first time that either an interstitial or a complex hydride can be formed starting from the same intermetallic compound. YMn_2D_6 is a paramagnet which follows a modified Curie–Weiss law. A NPD study from 1.5 to 290 K has confirmed the absence of long range magnetic order in YMn_2D_6.

In order to determine whether it was possible to prepare $ErMn_2H_6$ compounds, $ErMn_2$ was submitted to high hydrogen (deuterium) pressure like YMn_2. We succeeded in synthesizing $ErMn_2H_6$ ($ErMn_2D_6$) starting from C14 hexagonal $ErMn_2$, and investigated its structural and magnetic properties using XRD and NPD experiments as well as magnetic measurements. The thermal stability of this phase was also studied using differential scanning calorimetry (DSC) and thermal gravimetric analysis (TGA).

These new results are presented in this paper and discussed in relation to the structural and magnetic properties of the parent compound $ErMn_2$, its related hydrides and YMn_2D_6.

2. Experimental details

$ErMn_2$ was prepared by induction melting of the pure elements (Er, 99.9% and Mn 99.99%) followed by an annealing treatment for 11 days at 1073 K. The homogeneity of the sample was checked by XRD and electron probe microanalysis (EPMA).

The intermetallic compound was found to be homogeneous and of single phase. It crystallized in a hexagonal C14 structure with $a = 5.295(1)$ Å and $c = 8.645(1)$ Å. About 4 g of $ErMn_2D_6$ was prepared for the NPD experiments under 50 MPa deuterium pressure at 543 K.

Density measurements have been performed using a volumetric method with an Accupyc 1330 picnometer from Micromeritics Company.

The XRD patterns were measured with a D8 Brucker diffractometer equipped with a rear graphite monochromator in the range $10° < 2\theta < 120°$ with a step of 0.02° using

Table 1. Crystallographic data of RMn_2D_6 compounds (R = Y, Er) determined by XRD at room temperature.

Compound	a (Å)	c (Å)	V (Å^3)	Z	V/Z (Å^3)	$\Delta V/V$(%)
YMn_2	7.6791(1)		452.82	8	56.603	
YMn_2D_6	6.7084(1)		301.89	4	75.473	33.33
$ErMn_2$	5.2950(1)	8.6446(1)	209.90	4	52.475	
$ErMn_2D_6$	6.6797(1)		298.04	4	74.510	42.00

Table 2. Refined atomic positions (x, y, z), occupation number (N), Debye–Waller factor (B), line width parameters (U, V, W, Y), unit cell parameter (a), cell volume (V) and reliability factors (R_I, R_{wp}, R_{exp}, χ^2) for $ErMn_2D_6$ ND pattern measured on 3T2 at 300 K. The total occupation number for the Er and Mn1 atoms on the 8c site was fixed to 1 and the thermal B factors were constrained to be identical for the Mn1 and Mn2 atoms.

Atoms	Wyckoff position	x	y	z	N	B (Å^2)
Er	8c	0.25	0.25	0.25	0.500(1)	0.03(6)
Mn1	8c	0.25	0.25	0.25	0.500(1)	0.46(7)
Mn2	4a	0.0	0.0	0.0	1	0.46(7)
D	24e	0.2457(1)	0.0	0.0	1	2.10(3)
Line width: $U = 0.972$, $V = -0.137$, $W = 0.58$, $Y = 0.248$						
Space group: $Fm3m$ (216)						
Lattice parameters: $a = 6.6774(1)$ Å, $V = 297.7(1)$ Å^3						
Agreement factors: $R_I = 9.2\%$, $R_{wp} = 2.86\%$, $R_{exp} = 1.8\%$, $\chi^2 = 2.5$						

Cu Kα radiation. The NPD patterns of the deuteride were registered at 290 K on the 3T2 diffractometer and at temperatures varying between 1.5 and 290 K on the G4.1 diffractometer at the Laboratoire Léon Brillouin (LLB) at Saclay. For the 3T2 experiment the wavelength was 1.225 Å and the angular range $6° < 2\theta < 125°$ with a step of 0.05°. For the G4.1 experiments the wavelength was 2.427 Å and the angular range was $2° < 2\theta < 82°$ with a step of 0.1°. The deuteride was contained in a vanadium sample holder. All the XRD and NPD patterns were refined with the Rietveld method, using the Fullprof code [17]. The line shapes were refined with a Pearson VII function. The constraints of the refinement are given in the caption to table 2.

The magnetic measurements in both AC and DC modes were performed using a Quantum Design physical properties measurements system (PPMS) operating up to 9 T. Additional magnetization measurements were performed with a magnetometer of the High Magnetic Field Laboratory operating up to 23 T.

DSC measurements were performed on a TA-Q100 DSC apparatus from TA Instruments operating between 80 and 873 K. The sample holders were small aluminium pans covered but not sealed in order to allow escape of deuterium. TGA was performed on a Setsys Evolution 1750 balance from Setaram operating from 300 to 1500 K. The powder was placed in an open Pt crucible.

3. Results

3.1. X-ray and neutron diffraction

Despite the difference in crystal structure of the parent intermetallic compounds (C14 for $ErMn_2$ and C15 for YMn_2), $ErMn_2D_6$ crystallizes in the same FCC structure as YMn_2D_6 with a slightly smaller cell parameter (table 1). There are some weak additional lines in the

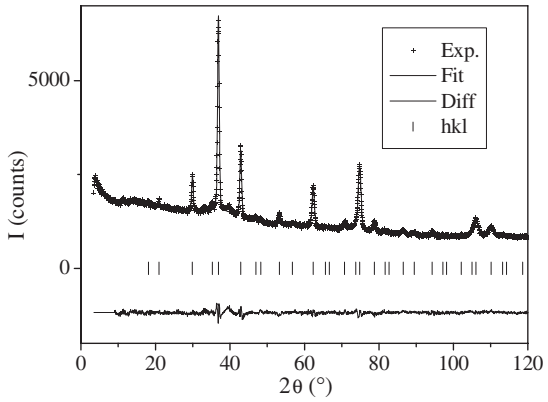

Figure 1. Experimental and refined NPD pattern of $ErMn_2D_6$ measured at 300 K on 3T2. The background slope is of instrumental origin.

XRD pattern that correspond to a small amount of $ErMn_2D_{4.2}$ (8%) and $ErMn_2D_{4.6}$ (1%). The relative cell volume variation ($\Delta V/V$) is significantly larger for $ErMn_2D_6$ than for YMn_2D_6 (table 1). The experimental density of $d = 6.59(10)$ g cm^{-3} is close to the one calculated for single phase $ErMn_2D_6$ ($d = 6.45$ g cm^{-3}). The larger cell volume increase for $ErMn_2D_6$ (42%) compared to YMn_2D_6 (33.3%) is surprising since in interstitial deuterides the volume expansion versus the D content is generally similar for isostructural compounds (see RFe_2D_5 compounds for example [12]). As the cell parameters of both RMn_2D_6 compounds are very close, this difference in $\Delta V/V$ indicates that they are less sensitive to the lanthanide contraction than their parent RMn_2 compounds. As this will be discussed further this effect can be related to the partially disordered cation arrangement of R and Mn on the same crystallographic site.

The NPD pattern measured on 3T2 at room temperature was refined in the $Fm3m$ space group with a disordered occupation of the 8c site by the Er and half the Mn atoms, a full occupancy of the 4a site by the other Mn atoms and of the 24e site by D atoms like for YMn_2D_6 (table 2 and figure 1). Any trial to refine the XRD and NPD patterns in a structure with an ordering of the Er and Mn atoms led to very bad agreement factors. For example a refinement in the $F\bar{4}3m$ subgroup of $Fm3m$ with Er in the 4a site and Mn in the 4b and 4c sites led to $R_{Bragg} \approx 30\%$ for both XRD and NPD patterns. The NPD pattern also contains a few weak and broad additional lines belonging to $ErMnD_{4.2}$ according to [18]. These peaks are less visible than in the XRD pattern, indicating that this phase is mainly located at the surface of the sample.

However, it was apparent that the half-widths of the Bragg peaks were quite broad. The refinements with a Pearson VII function led to a large U parameter compared to a standard crystallized compound in both XRD and NPD patterns. For example $U = 0.001$ for $ErMn_2$ and $U = 1.264$ for $ErMn_2D_6$ measured on the same x-ray diffractometer. In the Pearson VII function, the enlargement of the U parameter corresponds to additional microstrains [17]. Since the Mn and Er atoms have very different atomic radii ($r_{Mn} = 1.40$ Å and $r_{Er} = 1.76$ Å), it is therefore not surprising that a random distribution of Er and Mn atoms induces large microstrains.

From 1.5 to 290 K, all the NPD patterns measured on G4.1 were refined in the same cubic structure without significant change of the relative peak intensities (figure 2). No magnetic line contribution indicating a magnetic long range order was observed from 1.5 to 290 K. However, the difference curve of the G4.1 NPD patterns at 1.5 and 30 K showed a variation of the background intensity below $2\theta = 15°$ ($d = 9.2$ Å) and a broad contribution centred

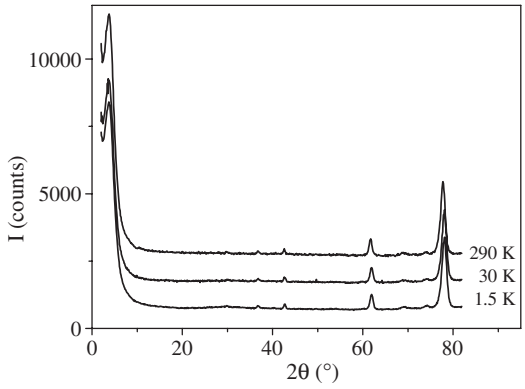

Figure 2. Experimental NPD patterns of $ErMn_2D_6$ measured on G4.1 at 1.5, 30 and 290 K.

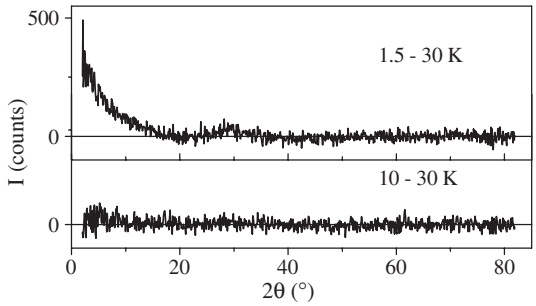

Figure 3. Difference NPD patterns of $ErMn_2D_6$ measured on G4.1.

at 30° ($d = 4.75(1)$ Å) (figure 3). These short range order contributions were still visible at 5 K with a lower intensity and disappeared at 10 K. The background decrease at low angles can be attributed to a short range order ferromagnetic contribution as observed in [19]. A fit of the intensity decrease below 15° assuming non-interacting spherical clusters with a uniform magnetization leads to a spherical radius of 13.5(5) Å, i.e. close to two nuclear cells. Additionally the broad peak centred at 4.75 Å that can be indexed in a cubic P mode should be attributed to a short range antiferromagnetic (AF) contribution. This value is close to the distance between either two Er (Mn1) atoms on the 8c site or two Mn2 atoms on the 4a site ($d_{M-M} = 4.723$ Å). For comparison we looked to see whether the same type of short range order was observed in the NPD pattern of YMn_2D_6, but the difference pattern between 1.5 and 30 K or any higher temperature did not show any additional contribution at low angle. This is an indication that the observed short range magnetic order is related to the Er moment (Er–Er or Er–Mn interactions). The cell parameter increased continuously with respect to temperature (figure 4).

3.2. Magnetic measurements

The magnetic results obtained for $ErMn_2$ are in good agreement with the literature [20–23]. The reverse susceptibility χ^{-1} of $ErMn_2$ and $ErMn_2D_6$ display the same behaviour from 290 K down to 150 K and diverge below 150 K (figure 5). The refinement of χ^{-1} with a Curie–Weiss law indicated similar effective moments ($\mu_{eff} = 10\ \mu_B$) but slightly different paramagnetic

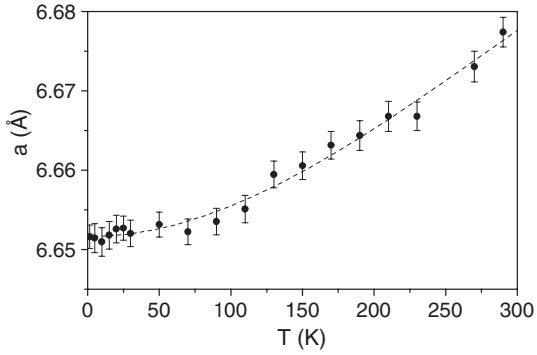

Figure 4. Cell parameter evolution measured by NPD on G4.1.

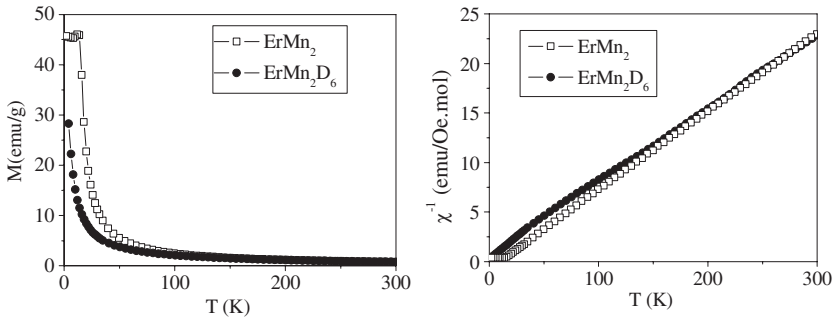

Figure 5. Magnetization and reverse susceptibility of $ErMn_2$ and $ErMn_2D_6$ ($B = 5$ kOe).

Table 3. Magnetic results of RMn_2 and RMn_2D_6 compounds (R = Y, Er)

Compound	T_C (K)	T_N (K)	M_s (μ_B) (4.2 K)	M_s (μ_B) (5 K)	θ_p (K)	μ_{eff} (μ_B)	χ (μ_B) $\times 10^6$ (290 K)
YMn_2		100				2.7	
YMn_2D_6				0.53	−30	2.0	1.07
$ErMn_2$	25		8.1		0	10.2	7.37
$ErMn_2D_6$	18		5		−11	10.2	7.92

temperatures θ_p (table 3). The isofield magnetizations also indicated different behaviour below 100 K. The Curie temperature of $ErMn_2D_6$ determined using the magnetization measured at 300 Oe is at $T_C = 18(2)$ K and slightly lower than in $ErMn_2$ (25 K). In addition, the $ErMn_2$ magnetization displayed a maximum at 15 K which was attributed to a canting of the Er spin and a minimum at 10 K due to a spin reorientation in agreement with [20]. For $ErMn_2D_6$ the isofield magnetization increased regularly down to 2 K and remained smaller than for $ErMn_2$.

The isothermal magnetization of $ErMn_2D_6$ deviated from linearity below 50 K, the analysis of the initial slopes lead to a Curie constant in agreement with those measured with the isofield magnetization. Comparison of the isothermal magnetizations of $ErMn_2$ and $ErMn_2D_6$ at 4.2 K and up to 230 kOe (figure 6(a)) showed that saturation is still not reached at 90 kOe for $ErMn_2D_6$ and that the value extrapolated at $B = 0$ ($M_s = 5$ μ_B) is lower than that of $ErMn_2$ (8.1 μ_B). However, the magnetization of $ErMn_2D_6$ was found to be several orders of magnitude

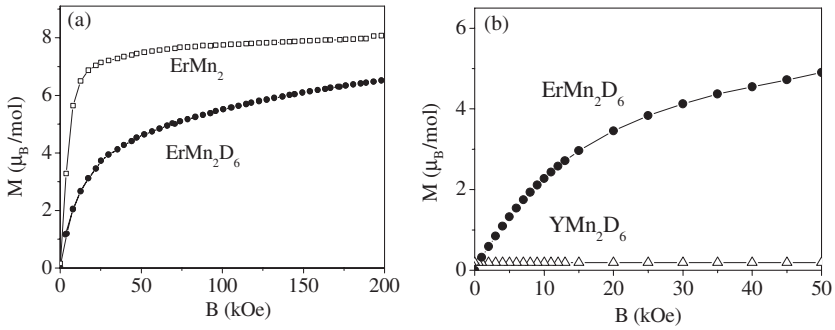

Figure 6. (a) Magnetization of $ErMn_2$ and $ErMn_2D_6$ at 4.2 K. (b) Magnetization of $ErMn_2D_6$ and YMn_2D_6 at 5 K.

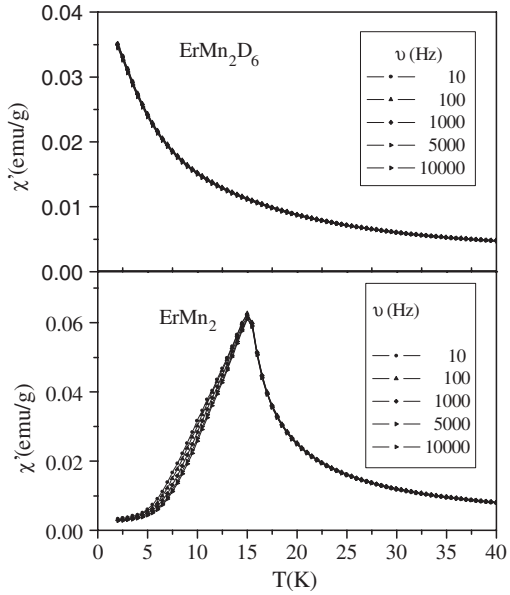

Figure 7. AC susceptibility for $ErMn_2$ and $ErMn_2D_6$ for various frequencies.

larger than that of YMn_2D_6 at 5 K (figure 6(b)); this confirms that the large magnetization observed at low temperature is related to the contribution of the Er moments.

AC susceptibility curves were measured at various frequencies for both $ErMn_2$ and $ErMn_2D_6$ (figure 7). $ErMn_2$ shows a maximum at 15 K related to the canting of the Er spins [20], whereas for $ErMn_2D_6$ the AC susceptibility increases continuously down to 4.2 K. This result confirms the absence of spin reorientation or spin glass behaviour in the deuteride.

3.3. Thermal stability

The DSC curve of $ErMn_2D_6$ was very similar to that of YMn_2D_6 (figure 8) [14]. The first peak at 523 K was attributed to the deuterium desorption of the remaining $ErMn_2D_{4.6}$ ($YMn_2D_{4.5}$) whereas the second intense peak at 668 K was attributed to the decomposition of RMn_2D_6 into RD_y and Mn (R = Y, Er). The TGA signal of $ErMn_2D_6$ (figure 9) indicates, a loss of mass of

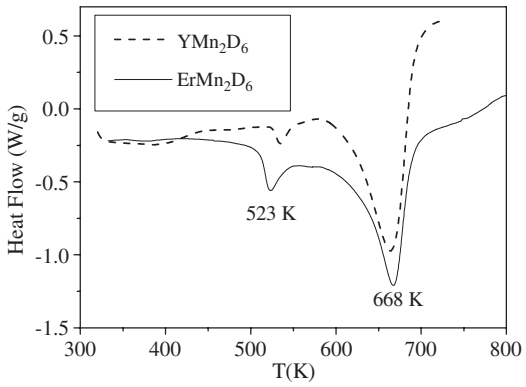

Figure 8. DSC curves of YMn_2D_6 and $ErMn_2D_6$ measured with a speed of 20 K mn^{-1}.

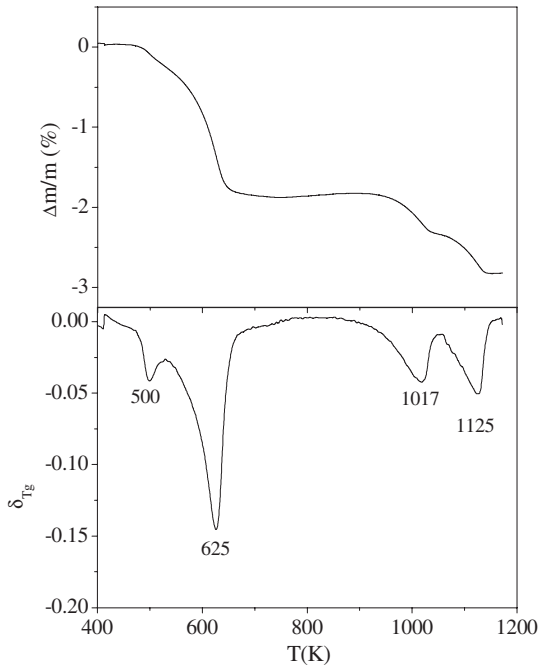

Figure 9. Relative loss of mass and signal derivative of the TGA measurement on $ErMn_2D_6$.

nearly 2% between 460 and 710 K corresponding to a total D desorption of 2.9 D/f.u. for both $ErMn_2D_{4.6}$ and $ErMn_2D_6$ compounds. The XRD pattern, after heating at 773 K in the TGA device, showed a mixture of ErD_2 and Mn. These results confirm the greater thermal stability of the RMn_2D_6 phases compared to the interstitial $RMn_2D_{4.6}$ phases.

Subsequent deuterium desorption was observed by TGA, with two peaks centred at 1017 and 1125 K in the derivative signal and a total weight loss of 1%. The XRD pattern obtained after heating at 1173 K displayed broad peaks of C14 $ErMn_2$. This suggests that the Er deuteride desorbs above 1000 K and that a recombination of Er and Mn atoms occurs next to form the parent C14 $ErMn_2$ compound again.

4. Discussion

The structural results obtained by XRD and NPD of $ErMn_2D_6$ indicate that this compound is isostructural to YMn_2D_6 [14] despite the different structures of their parent compounds. This study also confirms the disordered substitution of R and Mn atoms on the 8c sites. The contrast of the Er and Mn neutron scattering lengths is clearly large enough to exclude an ordered solution ($b_{Er} = 0.779$ barn and $b_{Mn} = -0.373$ barn). Additionally, the difference in the x-ray scattering coefficients between Er and Mn, which is larger than between Y and Mn, also shows that the disordered structure leads to a better refinement of the XRD pattern than an ordered one. It is also significant that the cell parameters of YMn_2D_6 and $ErMn_2D_6$ are very close and not as sensitive to the lanthanide contraction at would have been expected for an ordering of the R atoms.

The random occupation of Er and Mn atoms in the 8c site may result from the random displacement of the Er and Mn atoms that is required to transform a C14 or C15 type structure to a K_2PtCl_6 type one. In addition, the shortest distance between the Mn2 and the (Mn1, Er) atoms, 2.893 Å, is close to the average value of the Mn–Mn and Er–Mn distances in $ErMn_2$ (2.873 Å). The large microstrain contributions can therefore result from a broad local distance distribution.

$ErMn_2D_6$ displays the same thermal desorption behaviour as YMn_2D_6, with a decomposition into RD_2 and Mn at about the same temperature (668 K) (figure 8). This decomposition temperature is 100 K higher than that of the interstitial $RMn_2D_{4.6}$ phases in both cases. In addition, it has been observed that during synthesis the $ErMn_2D_6$ phase can be obtained at the expense of the $ErMn_2D_{4.6}$ phase: successive loading under high pressure increased the $ErMn_2D_6/ErMn_2D_{4.6}$ ratio. A subsequent two-step desorption of the Er deuteride was observed between 900 and 1150 K, leading to a recombination of Er and Mn to form C14 $ErMn_2$ again. Such hydride decomposition and recombination to form the starting intermetallic has already been observed for rare earth and iron alloys used as permanent magnets, through a hydrogenation–disproportionation–desorption–recombination (HDDR) process [24]. A recombination of Ce hydride and $CeNi_5$ to form $CeNi_2$ was also observed upon heating amorphous $CeNi_2H_4$ [25].

What is the possible explanation for the RMn_2D_6 complex hydrides being more stable than the $RMn_2D_{4.6}$ interstitial metal hydrides?

The Mn2–D distance at 1.647(2) Å is similar to that observed in YMn_2D_6 (1.654 Å). As discussed in [14], these short Mn2–D distances are typical of covalent bonding and the structure of the RMn_2D_6 compounds is close to M_2TH_6 complex hydrides [26]. In addition the M_2TH_6 compounds are described as complex anions TH_6^{4-} surrounded by a cage of divalent M^{2+} cations. Assuming the same 18-electrons rule as for YMn_2D_6, one should suppose that the Mn atoms surrounded by the D atoms (Mn2) are Mn^{I} whereas the Mn on the 8c site (Mn1) should be Mn^{II}, considering trivalent Er (Er^{III}). This complex will have the formula $(Er^{III}Mn^{II})^{5+}(Mn^{I}D_6)^{5-}$. However, as XAS measurements on YMn_2D_6 at the Mn–K and Mn-$L_{2,3}$ edges revealed that Mn remains closer to a metallic state than to a ionic state, the charge transfer between Mn and D atoms probably remains limited in these RMn_2D_6 phases. Further studies are still necessary to get a better understanding of the electronic structure of this compound.

The higher stability of complex hydrides compared to interstitial hydrides can be due to the larger binding energy between the metal and the hydrogen atoms in the former case. In the RMn_2 Laves phase structure the hydrogen atoms may occupy the 2R + 2Mn, R + 3Mn and Mn4 interstitials sites. Deuterium absorption in $ErMn_2$ at moderate pressure leads to the formation of $ErMn_2D_{4.2}$ and $ErMn_2D_{4.6}$ [18, 27, 28]. Both compounds retain the hexagonal

symmetry of the unit cell with an increase of the cell volume ($\Delta V/V = 25\%$ and 32% respectively). The NPD study shows a random localization of the D atoms in tetrahedral 2Er + 2Mn interstitial sites in $ErMn_2D_{4.2}$. Since in $ErMn_2D_{4.6}$, the additional 0.4 D atoms occupy 2Er + 3Mn bipyramids, formed by a pair of Er + 3Mn tetrahedra [18], this can explain its anomalous volume expansion (7% for 0.4 D) compared to the general volume increase per D atoms (25% for 4.2 D).

It is therefore expected that a further increase of D content should induce an additional filling of the 2Er + 3Mn or Er + 3Mn interstitial sites. This assumption is supported by the fact than in other Laves phases deuterides with large D content like $ErFe_2D_5$ [11] and ZrV_2D_6 [29] the filling of the R + 3M sites is observed above about 4 D/f.u. For example in ZrV_2D_6, which crystallizes in an orthorhombic structure, the deuterium atoms are almost fully ordered with 3 D in 2Zr + 2V and 3 D in Zr + 3V interstitial sites [29]. But the filling of these additional R + 3M sites requires a significant increase of energy compared to that of the 2R + 2M sites. In addition, $ErFe_2D_5$ and ZrV_2D_6 are not very stable as they desorb deuterium within a few hours or days when stored at room temperature and without poisoning the surface. The lower stability of the R + 3M sites compared to 2R + 2M sites can be explained by the weaker hydrogen affinity for M atoms compared to R atoms. The lowered H affinity can be deduced from the enthalpy of formation of the binary hydrides: -114 kJ mol^{-1} for YH_2, -112 kJ mol^{-1} for ErH_2, -82 kJ mol^{-1} for ZrH_2, -35 kJ mol^{-1} for $VH_{0.5}$ and -8 kJ mol^{-1} for $MnH_{0.5}$ [30, 31]. In addition, since the difference of enthalpy of formation between $ErH_2(YH_2)$ and $MnH_{0.5}$ is larger than that between ZrH_2 and $VH_{0.5}$, the Er +3Mn sites will be less stable than the Zr + 3V sites. Therefore the formation of the complex deuteride should be favoured compared to an interstitial metal deuteride with unstable R + 3M sites.

The experimental results show that despite the ferromagnetic contribution observed in the magnetization isotherm at 4.2 K, no long range magnetic order is observed in the NPD patterns of $ErMn_2D_6$ down to 1.5 K. The two short range magnetic order contributions observed at 1.5 and 5 K correspond to both ferromagnetic (F) and antiferromagnetic (AF) interactions. As no long or short range magnetic order was observed for YMn_2D_6, this means that the local magnetic order is rather related to the contribution of the Er moments. In addition, the magnetization curve of $ErMn_2D_6$ at 4.2 K and 230 kOe is not saturated and the extrapolated saturation magnetization is significantly lower than that of $ErMn_2$.

Due to the random substitution of Er and Mn on the 8c site each Er atom has the same probability of having Er or Mn atoms as nearest ($d = 3.340$ Å) or second neighbours ($d = 4.723$ Å). The observation of short range magnetic order can be due to Er–Er interactions with F or AF coupling depending on the distances between the Er atoms. The slow increase of the magnetization versus applied field may be related to the energy necessary to return the Er spins which are AF coupled.

A large sensitivity of the magnetic order to the deuterium content in $ErMn_2D_x$ deuterides has already been observed for $x = 4.2$ and 4.6 [18, 27, 28]. The magnetic structures of the $ErMn_2$ deuterides are very sensitive to the difference of D content: in $ErMn_2D_{4.2}$ there are only short range order magnetic correlations whereas in $ErMn_2D_{4.6}$ sharp magnetic peaks related to an antiferromagnetic structure are observed. This large difference of magnetic structures has been related to the influence of the D atoms on the Mn sublattice and to the large influence of the local hydrogen environment on the first neighbour Mn–Mn interactions. In $ErMn_2D_{4.6}$, the Mn atoms form triangles with different types of magnetic interaction depending on the presence or absence of D atoms. The Mn atoms surrounded by D atoms form ferromagnetic triangles whereas those without D neighbours form antiferromagnetic triangles. In $ErMn_2D_{4.2}$, although the spin arrangement cannot be determined from the diffuse magnetic peak, it is expected that the D atoms located in the 2R + 2Mn interstitial sites are responsible for the breakdown of the

long range magnetic order. It is therefore interesting to notice that in $ErMn_2D_6$ the long range order is also broken, but probably due to the disordered (Er, Mn) substitution.

5. Conclusions

Applying high hydrogen pressure to hexagonal C14 $ErMn_2$ Laves phase allowed us to synthesize a novel $ErMn_2D_6$ phase. This compound is isostructural to YMn_2D_6, which crystallizes in a K_2PtCl_6 type structure in which the CaF_2-type metal substructure is partially disordered. This result indicated that the structure of the fluorite RMn_2D_6 compounds does not depend on the C15 or C14 structure of the parent RMn_2 compound.

$ErMn_2D_6$ has the same thermal stability as YMn_2D_6 which is about 100 K higher than for the $RMn_2D_{4.5}$ deuterides. Above 600 K $ErMn_2D_6$ decomposed in ErD_2 and Mn. Then above 1000 K a subsequent ErD_2 decomposition led to a recombination of Er and Mn in C14 $ErMn_2$. The magnetic measurements on $ErMn_2D_6$ indicated a ferromagnetic behaviour with $T_C = 18$ K and an extrapolated saturation magnetization of 5 μ_B at 4.2 K. Nevertheless, the neutron diffraction measurements revealed only a short range magnetic order below 5 K. The random substitution of the Er and Mn atoms on the 8c site was probably at the origin of the absence of long range magnetic order.

Acknowledgments

We are thankful to V Lalanne for the synthesis of $ErMn_2$ and E Leroy for the EPMA analysis. Thanks also to F Cuevas for his help in DSC experiments and to B Rieux for the NPD measurement on 3T2 spectrometer. This work has been performed in the frame of the CNRS-PAN agreement No 18248. S M Filipek gratefully acknowledges financial support from Grant No PBZ-KBN-117/T08/06. R S Liu and H D Yang also would like to thank the financial support from the National Science Council under the grant no. NSC 95-2113-M-002-003.

References

[1] Przewoznik J, Paul-Boncour V, Latroche M and Percheron-Guégan A 1995 *J. Alloys Compounds* **225** 436
[2] Przewoznik J, Paul-Boncour V, Latroche M and Percheron-Guégan A 1996 *J. Alloys Compounds* **232** 107
[3] Figiel H, Przewoznik J, Paul-Boncour V, Lindbaum A, Gratz E, Latroche M, Escorne M, Percheron-Guégan A and Mietniowski P 1998 *J. Alloys Compounds* **274** 29
[4] Figiel H, Zukrowski J, Gratz E, Rotter M, Lindbaum A and Markosyan A S 1992 *Solid State Commun.* **83** 277
[5] Latroche M, Paul-Boncour V, Percheron-Guégan A and Bourée-Vigneron F 1998 *J. Alloys Compounds* **274** 59
[6] Latroche M, Paul-Boncour V, Percheron-Guégan A, Bourée-Vigneron F and André G 2000 *Physica* B **276–278** 666
[7] Goncharenko I N, Mirebeau I, Irodova A V and Suard E 1997 *Phys. Rev.* B **56** 2580
[8] Goncharenko I N, Mirebeau I, Irodova A V and Suard E 1999 *Phys. Rev.* B **59** 9324
[9] Mirebeau I, Goncharenko I N and Golosovsky I V 2001 *Phys. Rev.* B **64** 140401
[10] Mondal S, Cywinski R, Kilcoyne S H, Rainford B D and Ritter C 1992 *Physica* B **180/181** 108
[11] Paul-Boncour V, Filipek S M, Marchuk I, André G, Bourée F, Wiesinger G and Percheron-Guégan A 2003 *J. Phys.: Condens. Matter* **15** 4349
[12] Paul-Boncour V, Filipek S M, Percheron-Guégan A, Marchuk I and Pielaszek J 2001 *J. Alloys Compounds* **317/318** 83
[13] Wang C-Y, Paul-Boncour V, Liu R-S, Percheron-Guégan A, Dorogova M, Marchuk I, Hirata T, Filipek S M, Sheu H-S, Jang L-Y, Chen J-M and Yang H-D 2004 *Solid State Commun.* **130** 815
[14] Paul-Boncour V, Filipek S M, Dorogova M, Bouree F, Andre G, Marchuck I, Percheron-Guegan A and Liu R S 2005 *J. Solid State Chem.* **178** 356
[15] Didisheim J-J, Yvon K, Fischer G and Shaltiel D 1980 *J. Less Common Met.* **73** 355
[16] Huang B, Bonhomme F, Selvam P, Yvon K and Fischer P 1991 *J. Less Common Met.* **171** 301

[17] Rodríguez-Carvajal J 1990 *Proc. Congr. Int. Union of Crystallography* p 127
[18] Makarova O L, Goncharenko I N, Irodova A V, Mirebeau I and Suard E 2002 *Phys. Rev.* B **66** 104423
[19] Hodges J A, Bonville P, Forget A, Yaouanc A, Dalmas de Reotier P, Andre G, Rams M, Krolas K, Ritter C, Gubbens P C M, Kaiser C T, King P J C and Baines C 2002 *Phys. Rev. Lett.* **88** 077204
[20] Talik E, Kulpa M, Mydlarz T, Kusz J and Bohm H 2003 *J. Alloys Compounds* **348** 12
[21] Makihara Y, Andoh Y, Hashimoto Y, Fujii H, Hasuao M and Okamoto T 1983 *J. Phys. Soc. Japan* **52** 629
[22] Marzec J, Przewoznik J, Zukrowski J and Krop K 1996 *J. Magn. Magn. Mater.* **157/158** 413
[23] Okamoto T, Nagata H, Fujii H and Makihara Y 1987 *J. Magn. Magn. Mater.* **70** 139
[24] Harris I R 1993 *Proc. 11th Workshop on Rare Earth Magnets and their Applications (Canberra, Australia)* p 347
[25] Paul-Boncour V, Lartigue C, Percheron-Guégan A, Achard J-C and Pannetier J 1988 *J. Less Common Met.* **143** 301
[26] Yvon K and Renaudin G 2005 Hydrides: solid state transition metal complexes *Encyclopedia of Inorganic Chemistry* 2nd edn, vol 3, ed R Bruce King (Chichester: Wiley) p 1814
[27] Viccaro P J, Shenoy G K, Niarchos D and Dunlap B D 1980 *J. Less Common Met.* **73** 285
[28] Makarova O L, Goncharenko I N and Le Bihan T 2004 *Solid State Commun.* **132** 329
[29] Bogdanova A N, Irodova A V, Andre G and Bouree F 2003 *J. Alloys Compounds* **356/357** 50
[30] Griessen R and Driessen A 1984 *Phys. Rev.* B **30** 4372
[31] Griessen R and Riesterer T 1988 Heat of formation models *Hydrogen in Intermetallic Compounds I; Topics in Applied Physics* vol 63, ed L Schlapbach (Berlin: Springer) p 219